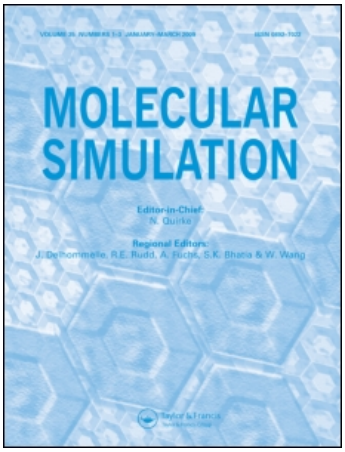

Molecular Simulation
Publication details, including instructions for authors and subscription information:
http://www.informaworld.com/smpp/title~content=t713644482

Simulation study of methanol and ethanol adsorption on graphitized carbon black

G. R. Birkett[a]; D. D. Do[a]
[a] Department of Chemical Engineering, University of Queensland, St Lucia, Qld, Australia

To cite this Article Birkett, G. R. and Do, D. D.(2006) 'Simulation study of methanol and ethanol adsorption on graphitized carbon black', Molecular Simulation, 32: 10, 887 — 899
To link to this Article: DOI: 10.1080/08927020601001911
URL: http://dx.doi.org/10.1080/08927020601001911

Molecular Simulation, Vol. 32, Nos. 10–11, 30 August–15 September 2006, 887–899

Taylor & Francis
Taylor & Francis Group

Simulation study of methanol and ethanol adsorption on graphitized carbon black

G. R. BIRKETT and D. D. DO*

Department of Chemical Engineering, University of Queensland, St Lucia, Qld 4072, Australia

(Received July 2006; in final form September 2006)

GCMC simulations are applied to the adsorption of sub-critical methanol and ethanol on graphitized carbon black at 300 K. The carbon black was modelled both with and without carbonyl functional groups. Large differences are seen between the amounts adsorbed for different carbonyl configurations at low pressure prior to monolayer coverage. Once a monolayer has been formed on the carbon black, the adsorption behaviour is similar between the model surfaces with and without functional groups. Simulation isotherms for the case of low carbonyl concentrations or no carbonyls are qualitatively similar to the few experimental isotherms available in the literature for methanol and ethanol adsorption on highly graphitized carbon black. Isosteric heats and adsorbed phase heat capacities are shown to be very sensitive to carbonyl configurations. A maximum is observed in the adsorbed phase heat capacity of the alcohols for all simulations but is unrealistically high for the case of a plain graphite surface. The addition of carbonyls to the surface greatly reduces this maximum and approaches experimental data with carbonyl concentration as low as 0.09 carbonyls/nm^2.

Keywords: Molecular simulation; Methanol; Ethanol; Adsorption; Carbon black

1. Introduction

The study of adsorption is a mature science with a large body of experimental work and theoretical study behind it. Currently the predominant field in the theoretical study of adsorption phenomena is in molecular simulation. The potential of molecular simulation to offer insight into molecular scale behaviour has been apparent since the very first simulation performed by Metropolis *et al.* [1]. Since this time, the popularity of molecular simulations has increased with increased computing power and improved methods with adsorption being just one field where it is applied.

Carbon adsorbents represent a major sub-category of adsorbents. Within the family of carbon adsorbents there is a wide range of characteristics from the complex structure of activated carbons to graphite and well defined nanotubes. Molecular simulation provides an appealingly direct way of understanding adsorption behaviour. In principle, if one is able to describe the interaction between fluid particles and that between a fluid particle and the adsorbent, it is possible to predict the amount adsorbed, the state of adsorbed molecules and the isosteric heat of adsorption [2]. This has been done with a large degree of success with non-polar molecules [3]. This has allowed for improved description of both pore size distributions and adsorption isotherms. Such confidence in adsorption simulations has yet to translate to strongly associating fluids.

Of the family of strongly associating fluids, water is the most important and widely studied. Simulation studies of water and carbon adsorbents have included studies of adsorption in homogeneous slit pores and nanotubes [4–8] and slit pores and nanotubes with functional groups [9–15]. However, there are many other important fluids that fall into the category of associating fluids including methanol and ethanol. Adsorption systems involving alcohols range from the removal of alcohols from aqueous streams to removing impurities from product alcohol streams. In addition to being industrially important, alcohols are interesting because they fall between non-polar fluids and water in the relative importance of coulombic to dispersive interactions. So the factors that effect alcohol adsorption are similar to those of water. So any model used to describe the adsorption of water on carbon black should be able to also describe the major features of alcohol adsorption. The adsorption of alcohols on

*Corresponding author. Tel.: + 61-7-3365-4154. Fax: + 61-7-3365-2789. Email: duongd@cheque.uq.edu.au

Molecular Simulation
ISSN 0892-7022 print/ISSN 1029-0435 online © 2006 Taylor & Francis
http://www.tandf.co.uk/journals
DOI: 10.1080/08927020601001911

carbons using molecular simulation has been scantly covered in the literature with only a few studies of adsorption in slit pores with water completed by Shevade *et al.* [16,17]. This paper will present the results of a simulation study of ethanol and methanol on a simple model of carbon black.

2. Potential models

2.1 Alcohol potential model

Rigid polyatomic models are used for methanol and ethanol. These models consist of Lennard-Jones (LJ) sites and partial charges. The potential energy between two alcohol molecules is given by equation (1).

$$u_{ij} = \sum_{a=1}^{A}\sum_{b=1}^{B}\frac{q_i^a q_j^b}{4\pi\varepsilon_0 r_{ij}^{ab}} + \sum_{c=1}^{C}\sum_{d=1}^{D}4\varepsilon_{ij}^{cd}\left[\left(\frac{\sigma_{ij}^{cd}}{r_{ij}^{cd}}\right)^{12} - \left(\frac{\sigma_{ij}^{cd}}{r_{ij}^{cd}}\right)^{6}\right] \quad (1)$$

where u_{ij} is the interaction energy between fluid molecules i and j, A and B are the number of charges on the molecules i and j, respectively, C and D are the number of LJ sites on the molecules i and j, respectively, ε_0 is the permittivity of a vacuum, r_{ij}^{ab} is the separation between the charge a on molecule i and the charge b on molecule j having charges q_i^a and q_j^b, respectively, and r_{ij}^{cd} is the separation between the LJ site c on molecule i and the LJ site d on molecule j with combined LJ well depth of ε_{ij}^{cd} and a combined LJ collision diameter of σ_{ij}^{cd} for the two sites. The values of ε_{ij}^{cd} and σ_{ij}^{cd} are given by Lorentz–Berthelot mixing rules in equations (2) and (3).

$$\varepsilon_{ij}^{cd} = \sqrt{\varepsilon_i^c \varepsilon_j^d} \quad (2)$$

$$\sigma_{ij}^{cd} = 0.5\left(\sigma_i^c + \sigma_j^d\right) \quad (3)$$

The alcohol models are characterised by the positions of the sites and the molecules and their LJ and Coulomb parameters. The methanol model used in this study is the "TraPPE-UA" potential presented by Chen *et al.* [18]. This is a model optimised for the phase co-existence of methanol based upon common parameters with other alcohols. This model, when originally proposed, took into account the effect of bond angle bending, but this has been assumed to be negligible and not taken into account for this paper. The model used for ethanol is that proposed by Schnabel *et al.* [19]. This is a rigid model of ethanol with the hydroxyl group in the trans configuration. This model has been optimised to reproduce the vapour–liquid equilibrium data of ethanol. The values of the molecular parameters for the methanol and ethanol models are given in table 1.

The vapour–liquid equilibrium properties of the two models have been calculated using Gibbs Ensemble Monte Carlo (GEMC) simulations [20,21] at 300 K. The GEMC simulations were conducted without any long range corrections for either the short ranged LJ interactions or the long ranged coulomb interactions. This was done for consistency since no long range corrections were used for the adsorption simulations (see below). This is in contrast with the original studies of the models [18,19] where long range corrections were taken into account. However, the vapour pressure of the models was almost negligibly affected by not using any long range correction. The properties of the two fluids at 300 K from GEMC are presented in table 2. The vapour pressures for methanol and ethanol agree well with the experimental values of 18.7 and 8 kPa, respectively.

Table 1. Molecular parameters of methanol and ethanol models.

Parameter	*Units*	*Methanol*	*Ethanol*
σ of CH_3	nm	0.375	0.36072
ε/k_b of CH_3	K	98.0	120.15
σ of CH_2	nm	–	0.34612
ε/k_b of CH_2	K	–	86.291
σ of O	nm	0.302	0.31496
ε/k_b of O	K	93.0	85.053
q of CH_3	e	0.265	–
q of CH_2	e	–	0.2556
q of O	e	−0.700	−0.69711
q of H	e	0.435	0.44151
R_{C-C}	nm	–	0.198420
R_{C-O}	nm	0.1430	0.171581
R_{O-H}	nm	0.0945	0.095053
Angle CCO	°	–	90.95
Angle COH	°	108.5	106.368

2.2 Carbon black

The simulation cell is bound in the z-direction by the walls of a slit pore. Only one of the walls of the pore has an attractive interaction with the fluid molecules. This pore wall interacts with a fluid molecule according to the Steele 10-4-3 potential [22] given by equation (4).

$$u_i^{\text{surf}} = \sum_{a=1}^{A} 2\pi\rho_s\varepsilon_{is}^a\left(\sigma_{is}^a\right)^2\Delta\left[\frac{2}{5}\left(\frac{\sigma_{is}^a}{z_i^a}\right)^{10} - \left(\frac{\sigma_{is}^a}{z_i^a}\right)^4 - \frac{{\sigma_{is}^a}^4}{3\Delta(z_i^a + 0.61\Delta)^3}\right] \quad (4)$$

where u_i^{surf} is the interaction between an alcohol molecule, i, and the carbon surface, A is the number of LJ sites on molecule i, ρ_s is the graphite's carbon density, Δ is the separation distance between graphite layers, z_i^a is the shortest distance between LJ site a and the surface and ε_{is}^a

Table 2. Saturation properties of methanol and ethanol models at 300 K from GEMC. Uncertainties of values are given in parentheses.

Parameter	*Units*	*Methanol*	*Ethanol*
P^{VAP}	Kpa	16.9 (1.5)	8.5 (1.0)
ρ^{V}	mol/m^3	8.4 (1.0)	3.4 (0.4)
ρ^{L}	Kmol/m^3	24.1 (0.1)	17.0 (0.1)
ΔH^{V}	kJ/mol	38.6 (1.0)	42.3 (0.4)
C_{V}^{c} liquid	J/mol K	44.5 (4.0)	55.0 (5.0)

Table 3. Molecular parameters of carbon surface used in the Steele 10-4-3 equation.

σ_{ss} (nm)	ε_{ss}/k_b (K)	ρ_s (nm^{-3})	Δ (nm)
0.34	28.0	114	0.335

and σ_{is}^{a} are the LJ well depth and collision diameter between site a and the surface calculated using equations (2) and (3), respectively. The molecular parameters for the carbon wall Steele potential are given in table 3.

The opposing wall has no attractive term and has only an effectively infinite repulsion for molecules that cross the pore wall. The simulation cell is repeated periodically in the x and y directions to approximate an infinite pore. The model pore has a width of 5.0 nm and a length in the simulation cell of at least 7.5 nm, with larger lengths sometimes used to increase the number of particles in the simulation to improve the reliability of heat capacity calculations. A simulation cell length 1.5 times the pore width has been observed to be sufficient by Jorge and Seaton [23] to avoid observable finite size effects and this has been the experience of the authors as well. A pore width of 5.0 nm allows a good approximation of carbon black with the opposing hard wall having no observable effect on the adsorption at the Steele potential surface until many layers are formed at pressures very close to the vapour pressure of the fluid.

2.3 Carbonyl functional groups

The only type of functional group considered in this study is carbonyl. This is modelled with a single LJ site at the oxygen a distance, R_{CO}, perpendicular to the carbon surface, a positive charge on the surface and negative charge at the oxygen. The parameters for the carbonyl group are taken from the OPLS potential model for amino acids [24] and are given in table 4.

The configuration of functional groups has previously been observed to strongly affect the adsorption behaviour of water [9,13] and ammonia [25]. This is expected to be the case for alcohols as well. The same configurations of carbonyls used to study this effect on ammonia are used here, with a range of grouped and evenly spread carbonyls. The different configurations used are presented in figure 1.

The interaction between alcohol molecules and the carbonyls is given by equation (1) with $A = 2$ and the LJ parameters given by the combination of their respective LJ parameters using the Lorentz–Berthelot mixing rule (equations (2) and (3)). Carbonyls, as opposed to other functional groups, were chosen for their simplicity and that carbonyls represent a large percentage of the functional groups on carbon blacks treated at high temperatures [26,27]. The simplicity of carbonyls offers a very small saving in computational cost compared with hydroxyl or carboxylic groups but more importantly, reduces the parameters that can be adjusted. Carbonyls can only be adjusted by their positions whereas hydroxyl and carboxyl groups must have their orientation specified. This combined with the fact that comparison is being made between simulation and experiments on carbon blacks heat treated at high temperatures makes carbonyl a good choice for this preliminary study.

Table 4. Molecular parameters of carbonyl group.

ε/k_b (K)	σ (nm)	q^- (e)	q^+ (e)	R_{CO} (nm)
105.8	0.296	−0.5	0.5	0.1233

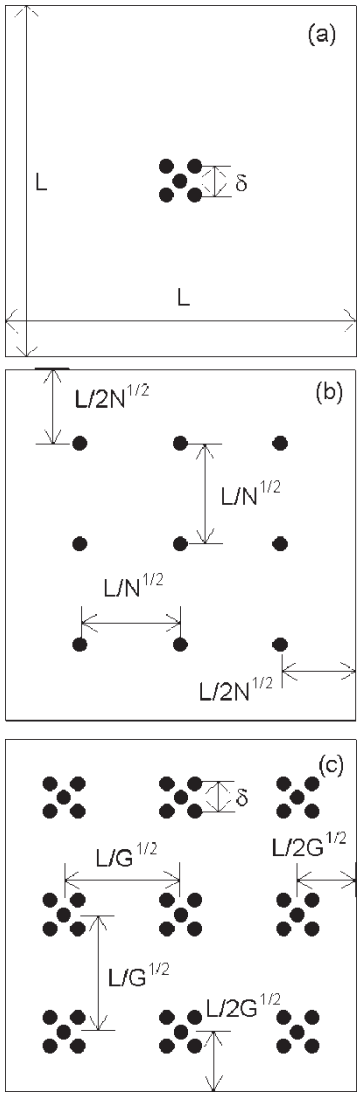

Figure 1. Configurations of carbonyls (•) on the bottom plane of the pore (a) group of five carbonyls located at the centre of the pore wall, (b) evenly spaced single carbonyls and (c) evenly spaced groups of five carbonyls. δ, the characteristic separation of a group of five carbonyls; L, simulation cell box length in x and y axis; N, the number of evenly spaced carbonyls; and G, the number of groups of five carbonyls.

3. Simulation methodology

Monte Carlo simulations were conducted using the GCMC ensemble [28]. For some isotherm points, the aggregation-volume-bias (AVB) sampling proposed by Chen and Siepmann [29] was used. In this simulation study we used the scheme termed AVBMC2 by Chen and Siepmann [29].

We will refer to a move performed under the AVBMC2 scheme as an AVB move. The chemical potentials used in the simulations were the ideal chemical potential of the pressures reported, a reasonable approximation for the low pressures studied. Simulations were conducted at 300 K at pressures from 0.001 to 12 kPa for methanol ($P^{VAP} = 16.9$ kPa) and from 0.0005 to 7 kPa for ethanol ($P^{VAP} = 8$ kPa). Each simulation isotherm point was equilibrated until the number of molecules and energy of the system reached a stable value. From this point ensemble data was collected over a minimum of 2.5×10^7 up to 6×10^9 Monte Carlo steps, depending on the point on the isotherm. Steps were either translations, rotations, insertions, deletions or AVB moves. AVB moves were only used at low coverage where the sampling of clusters is extremely important for the calculation of isosteric heats and heat capacities. When they were used, the number of attempted AVB moves was set to achieve one successful swap per 100 moves. If this could not be achieved, the maximum number of AVB moves was set to five times the number of translations and rotations. The number of insertions was set to give four successful insertions per 100 moves. If this could not be achieved, the maximum number of insertions was set to five times the number of translations and rotations. The number of deletions was set equal to the number of insertions. Once an isotherm point is completed, its final configuration is used as the initial configuration of the next isotherm point, mimicking the experimental adsorption procedure. Uncertainties of ensemble averages are estimated by calculating the variance of the ensemble quantities when they are broken into 10 evenly sized blocks. Uncertainties presented as error bars in figures hereafter are the variances calculated by this technique.

No long-range corrections were used for either dispersion (LJ) or electrostatic interactions. This is due solely to the greatly increased computation time required for isotherms using appropriate long range corrections for the coulomb interactions like the technique of Heyes and Van Swol [30,31] or a two-dimensional Ewald-type sum [31,32]. Shevade *et al.* [16] have reported a small difference in the potential of adsorption systems between using a long range correction, a two-dimensional Ewald type [32], and ignoring the long range corrections. Citing an increase in computational cost of two orders of magnitude, long range corrections were not used by Shevade *et al.* [16]. Long range corrections have not been used for many other simulation studies of water in carbon pores [4–8]. LJ interactions were cut at a cylindrical cut-off in the x–y plane at a distance R_c. Coulomb interactions were cut on a molecular basis using the separation of specific atom sites on the molecules (oxygen in methanol and the CH_2 group in ethanol). So if two molecules satisfied this cut-off criterion, all Coulomb interactions were counted between the particles even if some charge separations were greater than R_c in the x–y plane. Cut-offs on an atomistic charge–charge basis would lead to spuriously high interactions in the case where not all charges on a molecule are used in the interaction potential calculation. The same cut-offs were applied to the interactions of alcohol molecules with carbonyl sites. For comparison with experiments conducted in the literature, the isosteric heat was calculated for all simulations. The isosteric heat was calculated using equation (5) [2].

$$q_{st} \cong \frac{\langle NU \rangle - \langle N \rangle \langle U \rangle}{\langle N^2 \rangle - \langle N \rangle \langle N \rangle} + kT \tag{5}$$

The first term in equation (5) can also be split into the different contributions of the system potential energy U. The three contributions to the potential energy are the fluid–fluid interactions, the fluid–surface interactions and the fluid–functional group interactions. Replacing U in equation (5) with one of these contributions to the potential, and discounting the second term, will give its contribution to the isosteric heat [33]. The heat capacity of the adsorbed alcohols was also calculated. The configurational (i.e. ignoring kinetic contributions) component of the constant volume heat capacity, C_V^c, is calculated using equation (6) [28].

$$C_V^c = \frac{(\langle U^2 \rangle - \langle U \rangle \langle U \rangle) - \frac{(\langle UN \rangle - \langle U \rangle \langle N \rangle)^2}{\langle N^2 \rangle - \langle N \rangle \langle N \rangle}}{\langle N \rangle k_b T^2} \tag{6}$$

4. Results

The first series of results presented in figures 2 and 3 are simulation isotherms at 300 K for methanol and ethanol, respectively. The different isotherms for each alcohol are for different carbonyl configurations. In figures 2 and 3 there are isotherms for the case of no carbonyls, five carbonyls (figure 1(a) with $\delta = 0.3$ nm), 49 evenly spaced carbonyls (figure 1(b)) and nine evenly spaced groups of five carbonyls (figure 1(c) with $\delta = 0.3$ nm).

Figures 2 and 3 show a number of features. For most isotherms, for both ethanol and methanol, the initial adsorption is quite low. A pressure is then reached where the adsorption uptake increases quickly with respect to pressure. This uptake is much sharper for methanol where

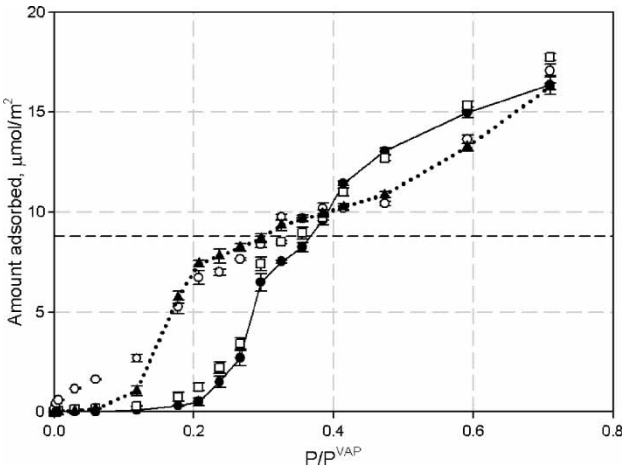

Figure 2. Simulation isotherms for methanol at 300 K on a carbon surface with: no carbonyls (filled circles with solid line), five carbonyls separated by $\delta = 0.3$ nm (empty squares), 49 evenly spaced carbonyls (filled triangles with dotted line) and nine evenly spaced groups of five carbonyls with $\delta = 0.3$ nm (empty circles). Horizontal dotted line indicates monolayer coverage. Lines are a guide for the eye only.

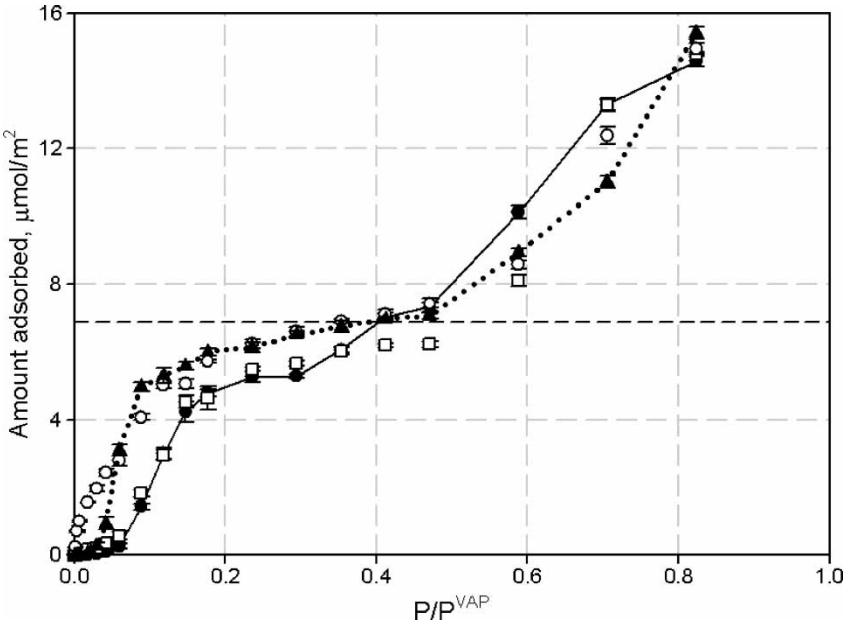

Figure 3. Simulation isotherms for ethanol at 300 K on a carbon surface. Symbols as per figure 3.

it occurs at a higher reduced pressure. The uptake slows and the isotherm goes through a point of inflection. The uptake continues to slow until approximately monolayer coverage is reached. The monolayer coverage indicated in figures 2 and 3 was calculated using the density distribution, with respect to perpendicular distance from the carbon surface, when adsorption was well above monolayer coverage at a pressure of 12 kPa for methanol and 7 kPa for ethanol. The density distributions for the methyl groups of methanol and ethanol, at these respective pressures, are given in figure 4. The density distribution of the methyl group was chosen because it has the greatest affinity to the surface leading to the clearest density peaks to define the first and second layers.

Figure 4 shows that the density distributions of the methyl groups for ethanol and methanol are fairly typical for sub-critical adsorption. The monolayer coverage is calculated by integrating the area under the first peak. The upper limit of this integration is assigned as where the minimum occurs between the first and second peaks in the distribution. This is shown by the arrows in figure 4. Using this technique, the monolayer adsorption for methanol and ethanol is 8.8 and 6.65 μmol/m^2, respectively. These monolayer coverages correspond to molecular projection areas of 18.8 and 25.0 Å^2 for methanol and ethanol, respectively. This is quite comparable to the projection areas of 16 and 22 Å^2 [34] calculated from van der Waal's

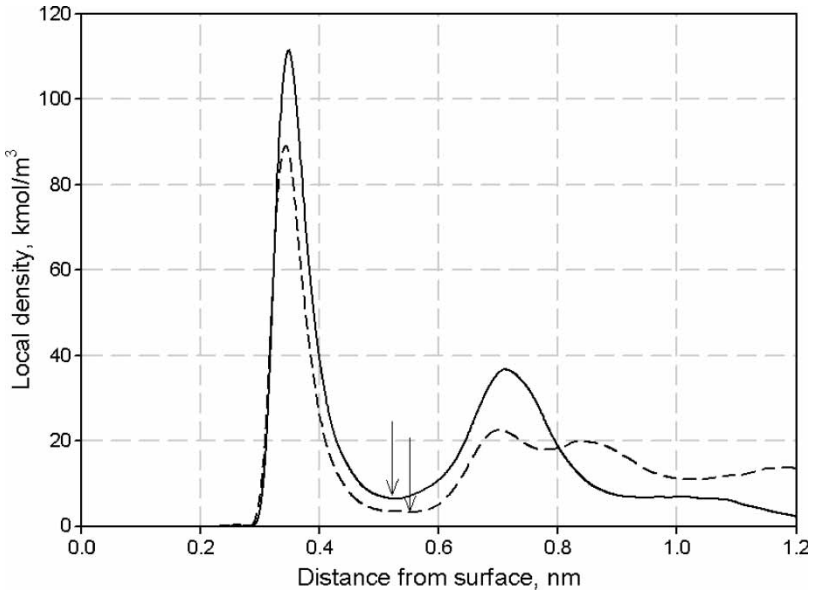

Figure 4. Density distribution, perpendicular to carbon surface, for methanol (solids line) and ethanol (dashed line) methyl groups at 300 K and pressures of 12 and 7 kPa, respectively. Arrows indicate the limit of the integration for calculating monolayer coverage.

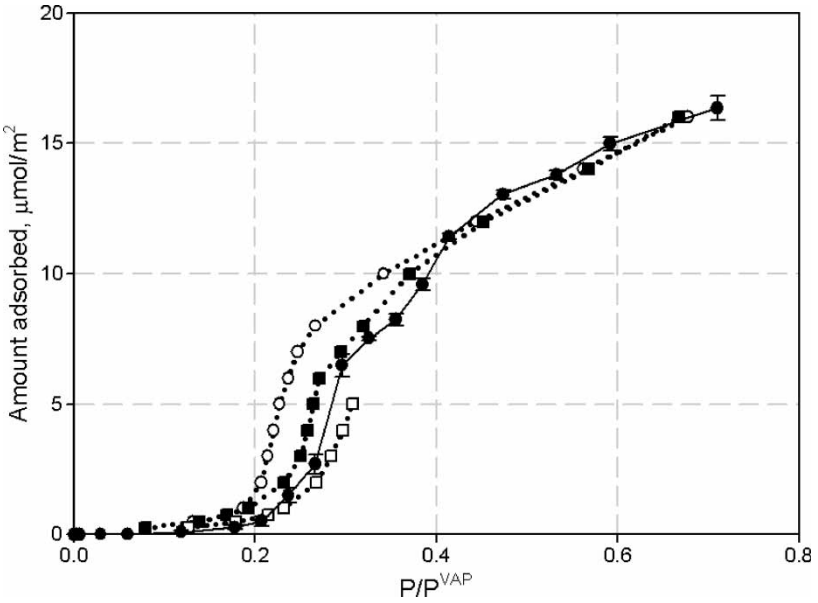

Figure 5. Experimental adsorption isotherms for methanol on carbon black at various temperatures [34]: 273.15 K (empty circles with dotted line), 293.15 K (filled squares with dotted line) and 326.15 K (empty squares with dotted line). Simulation results at 300 K (filled circles with solid line) for a surface with no carbonyls. Pressure reduced by the corresponding vapour pressure at that temperature. Lines are a guide for the eye only.

dimensions at 293.15 K. From monolayer coverage onwards, the behaviour of all isotherms is much the same with adsorption slightly affected by large concentrations of carbonyl groups on the surface. For both ethanol and methanol, the presence of carbonyl groups increases the adsorption at lower pressures (prior to monolayer coverage). A large number of evenly spaced carbonyls (plot for 49 carbonyls in figures 2 and 3) or a large number of groups of carbonyls (plot for nine groups of carbonyls in figures 2 and 3), significantly changes the isotherm, from that of the bare surface. Groups of five carbonyls provide the greatest increase in adsorption with each of the five sites acting as a site of high affinity for methanol and ethanol. The results of the simulations on the bare graphitic surface are compared against the experimental results available in the literature in figures 5 and 6 for methanol [34] and ethanol [35,36], respectively.

Figures 5 and 6 show a fair agreement between the simulation results and the experimental data. The methanol simulation in figure 5 follows the trend of isotherms with increasing temperature and matches the shape of the experimental isotherms very well. The ethanol adsorption does not agree as well with the experimental data but the experimental data available does

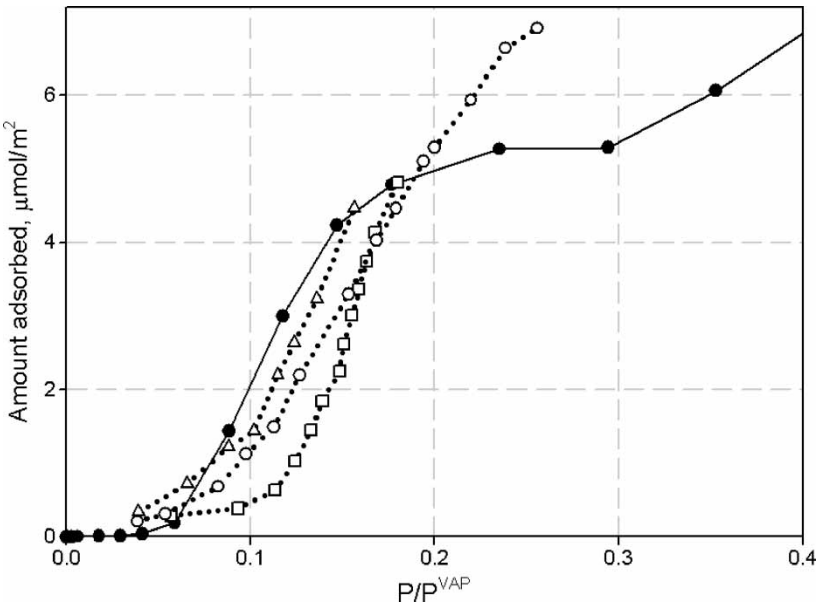

Figure 6. Experimental adsorption isotherms for ethanol on carbon black at various temperatures [35,36]: 278.15 K (empty squares with dotted line); 293.15 K (empty triangles with dotted line); and 307.15 K (empty circles with dotted line). Simulation results at 300 K (filled circles with solid line) for a surface with no carbonyls. Pressure reduced by the corresponding vapour pressure at that temperature. Lines are a guide for the eye only.

not appear to be consistent either with no clear shifting of the adsorption isotherm to higher or lower reduced pressures with temperature (as opposed to methanol in figure 5). Putting this anomaly aside, the shape of the experimental isotherms is quite consistent with higher temperatures leading to shallower isotherms. The simulation isotherm continues this trend and appears to give a reasonable approximation of the experimental isotherm. So the bare surface model of the carbon gives a reasonable approximation of the experimental data. This is also true for simulations with small numbers of carbonyls, such as the isotherms for the five grouped carbonyls and $\delta = 0.3$ nm shown in figures 2 and 3. So it is not possible to differentiate between a surface with a small number of functional groups and that without using the experimental isotherms at reduced pressures greater than 0.05. By contrast the isotherms for the surfaces with a large number of carbonyls, like isotherms for the 49 evenly spaced carbonyls in figures 2 and 3, are clearly different from the experimental isotherms and cannot be a viable model of the heterogeneity of the carbon surface. Now we can look at the heats of adsorption for the methanol and ethanol systems. Shown in figure 7 are the heats of adsorption for ethanol and methanol for surfaces with no functional groups and with a group of five carbonyls. Note that the isosteric heats in figure 7 are for loadings considerably less than the monolayer coverage of 8.8 and 6.65 μmol/m^2 for methanol and ethanol, respectively.

Figure 7 represents the sample range of behaviour possible for the isosteric heat of alcohol on carbon black. A system with no functional groups will start with an isosteric less than the heat of vaporization before rising to be approximately equal to the heat of vaporization. With a suitable configuration of functional groups, such as five carbonyls separated by 0.3 nm, the heat of adsorption starts well above the heat of vaporisation before dropping to a minimum and then increasing again to be slightly greater than the heat of vaporization. The heats of adsorption for the surfaces with and without functional groups converge at very low coverage. This suggests that the functional groups contribute very little to the heat of adsorption above a surface coverage of approximately 0.5 μmol/m^2 (equivalent to 6% of monolayer coverage). From this point onwards it would appear the mechanism of adsorption is the same for both the surfaces with and without functional groups. To further investigate this, the isosteric heat from equation (5) can be split into its contributions from fluid–fluid, fluid–solid and fluid-functional group interactions. The results of doing this for methanol on a surface with five functional groups are presented in figure 8.

In figure 8 we see that the isosteric heat, for a surface with closely grouped carbonyls, is dominated initially by the fluid–functional group contributions and the fluid–solid contributions. As loading increases to 0.5 μmol/m^2, the fluid–functional group contributions decrease quickly to become negligible, the fluid–fluid contributions increase and the fluid–solid contributions remain steady. The invariance of the fluid–solid contributions indicates adsorption only in the first layer. At higher coverages, where multiple layers start to form, the fluid–surface contributions decay and the isosteric heat is increasingly dominated by the fluid–fluid contributions. However, the isosteric heat remains essentially unchanged through to multilayer coverage even though the underlying contributions change significantly. For different carbonyl configurations, the isosteric heat alters only by changes in the contribution from the fluid–functional group interactions. Initial isosteric heats greater than the heat of vaporization are only possible if the carbonyls are grouped

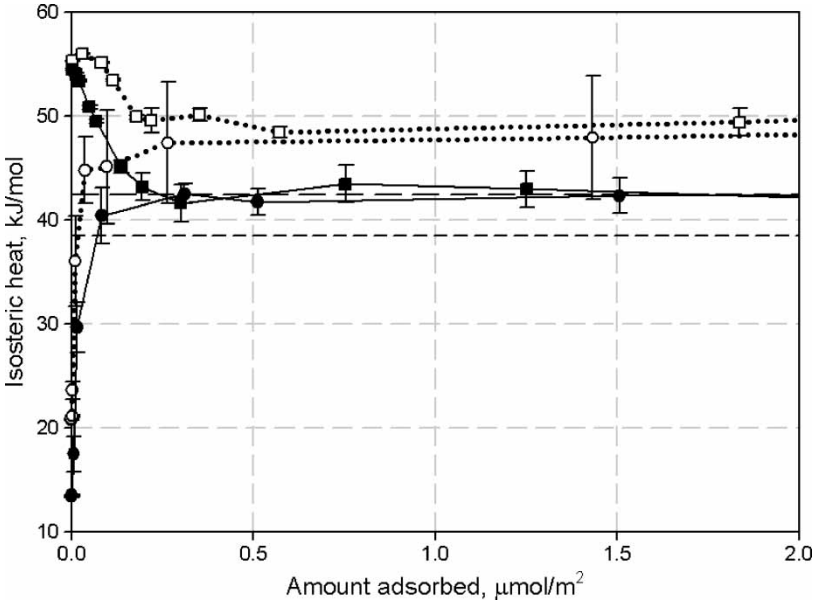

Figure 7. Heats of adsorption from simulations for methanol (filled symbols with solid lines) and ethanol (empty symbols with dotted lines) with a surface having no carbonyls (circles) and a surface with a five centre configured carbonyls and $\delta = 0.3$ nm (squares). Lines are a guide for the eye only. Horizontal short dashed and long dashed lines indicate the heats of vaporization of the methanol and ethanol models, respectively.

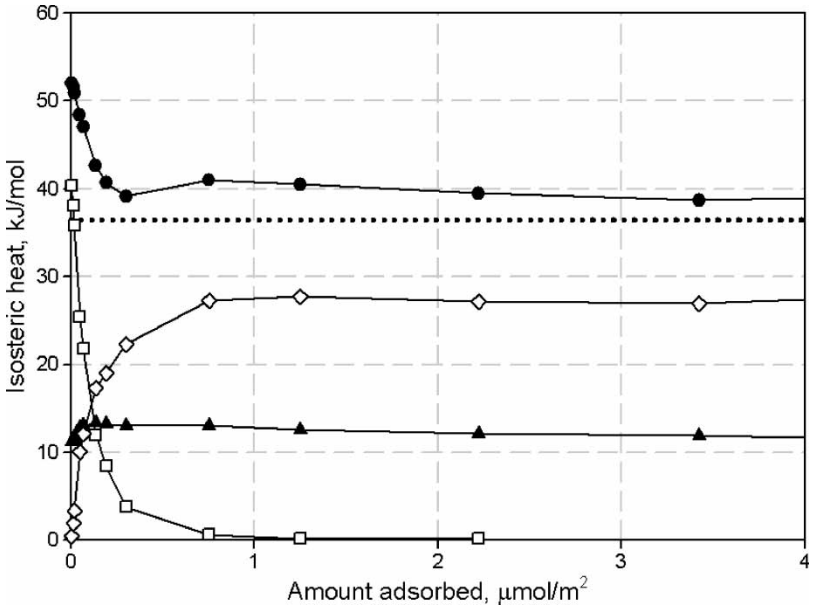

Figure 8. Heats of adsorption for methanol on a surface with a single group of five carbonyls separated into its contribution from: fluid–carbonyl interactions (empty squares), fluid–surface interactions (filled triangles), fluid–fluid interactions (empty diamonds) and the total configurational contribution to the isosteric heat (filled circles). Solid lines are a guide for the eye. Horizontal dotted line indicates the heat of vaporization.

very close together. Nearly identical behaviour is seen in the isosteric heat for ethanol. The major difference between the isosteric heats for ethanol and methanol is that ethanol has a greater fluid–solid contribution by approximately 7 kJ/mol. This is a result of the additional dispersion site (CH_2) of the ethanol compared with methanol. The similarity of the fluid–fluid and fluid–functional group contributions to the isosteric heat for methanol and ethanol suggests that mode of adsorption of the two is similar. Figures 9 and 10 show snapshots of the configuration from the simulations for methanol, at 4.5 kPa, and ethanol, at 0.75 kPa, respectively. These two pressures were chosen since they gave a similar relative adsorption, compared with monolayer coverage, of about 20%, for both systems.

Figures 9 and 10 show the tendency of both methanol and ethanol to form a significant number of hydrogen bonds. Closer inspection shows a tendency not just to bond, but to form tetramers for both methanol and ethanol. The tetramers form an approximately square with the oxygen located at the corners and the hydrogen along its side. Favouring such a configuration should be visible in the radial distributions [28] of the system. The oxygen–oxygen (O—O) and oxygen–hydrogen (O—H) radial distributions for methanol and ethanol, at the same pressures as figures 9 and 10, are

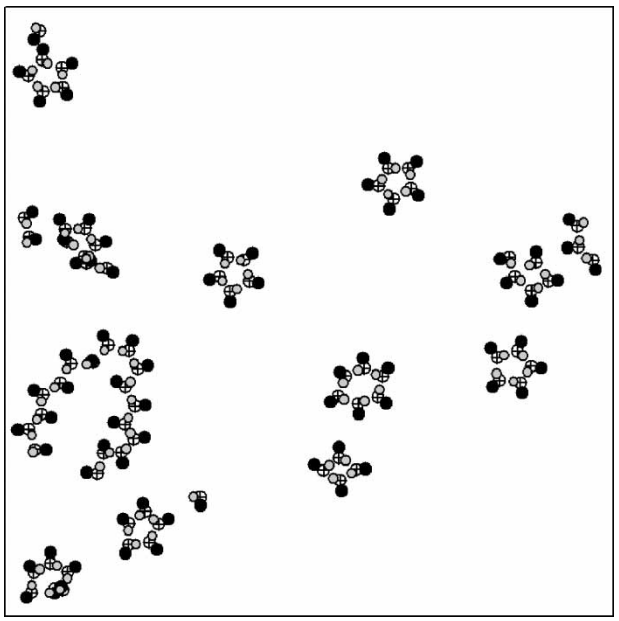

Figure 9. Snapshot of methanol positions on bare carbon black for a simulation performed at 300 K and a reduced pressure of 0.27. Different groups are represented: CH_3 (black); O (cross); and H (gray).

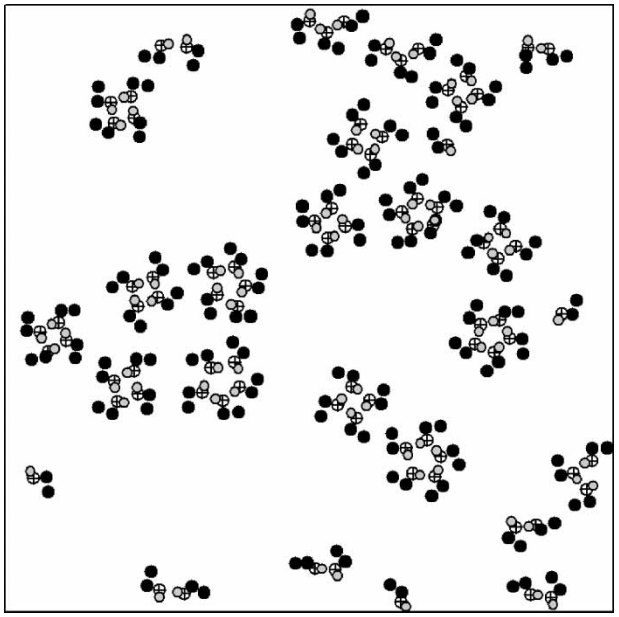

Figure 10. Snapshot of ethanol positions on bare carbon black for a simulation performed at 300 K and a reduced pressure of 0.09. Different groups are represented: CH_3 and CH_2 (black); O (cross); and H (gray).

presented in figure 11. The O—H distribution is between oxygen of one molecule and hydrogen of another molecule.

The radial distributions in figure 11 approximately correspond to strong hydrogen bonding with significant tetramer structures, as observed in figures 9 and 10. The stronger and more quickly decaying second peaks in both the O—O and O—H distributions for ethanol indicate that the tetramer structures are more prevalent for ethanol than methanol. One of the most interesting aspects of the adsorption of alcohol on carbon black is that the heat capacity of the adsorbed alcohol has a very distinct maximum, much greater than the saturated liquid's heat capacity [35]. The configurational component of the adsorbed alcohol's heat capacity was calculated using equation (6). The configurational part of the saturated liquid heat capacity (listed in table 2) is taken away from the adsorbed phase's to give what should be an absolute difference between the adsorbed phase heat capacity and the saturated liquid heat capacity. This relies on the assumption that the non-adsorbed gas phase in the simulations contributes negligibly to the results from using equation (6) and that the kinetic contributions to the heat capacity are the same for the adsorbed and liquid phases. This makes it possible to compare simulation and experiment results. We will term this quantity as the excess heat capacity for discussion hereafter. The excess heat capacities for methanol and ethanol for several carbonyl configurations are presented in figures 12 and 13. Figure 13 also includes experimental measurements of the excess heat capacity of ethanol on carbon black at 307.15 K [35]. No experimental results were available for the heat capacity of methanol on carbon black.

Figures 12 and 13 show that the simulations all have a maximum in the excess heat capacity. It also shows that for both ethanol and methanol, the greatest and sharpest maximum is for the surface with no functional groups. In the case of ethanol, this is far in excess of the heat capacity seen experimentally. The addition of functional groups reduces the magnitude of the maximum for both methanol and ethanol. Just as closely grouped carbonyls have the largest effect on the isosteric heat, they also cause the largest reduction in the excess heat capacity, compared with a similar number of relatively far spaced carbonyls. A small amount of heterogeneity can change the unrealistic heat capacity curve to that which is closer to experimental data. So the heat capacity curve is more sensitive to the addition of a small number of carbonyls than the adsorption isotherm (comparing the results of a surface with no carbonyls and one with five and $\delta = 0.3$ nm in figures 3 and 13). The surface with five carbonyls corresponds to a surface density of 0.09 carbonyls/nm^2. This is quite a low concentration to have such a significant effect on an experimentally observable quantity like the heat capacity. The sensitivity of the heat capacity to heterogeneity may provide an interesting tool (experimental data withstanding) of characterising adsorption behaviour on carbon black. Only one type of heterogeneity, carbonyl groups, has been considered here. It would be of interest for future studies to see how the heat capacity is affected by other functional groups, surface defects and the finite extent of surfaces. The peak in the heat capacity of alcohol on a carbon black surface appears to arise from fluid–fluid bonding in the adsorbed layer. This can be investigated using the radial distribution, $g(r)$, of the system. Now we define a clustering parameter, CP,

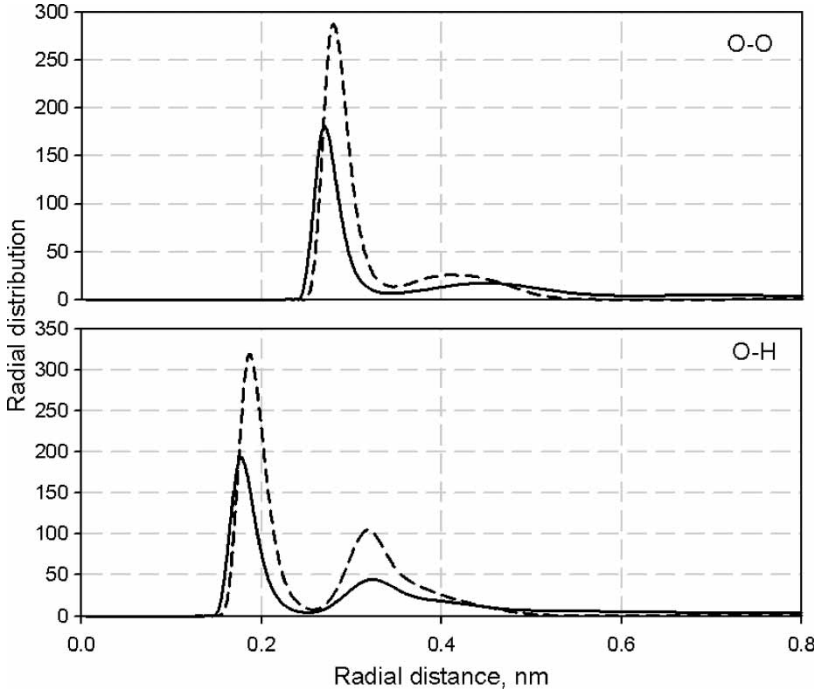

Figure 11. O—O and O—H radial distributions for methanol (solids lines) and ethanol (dashed lines) at 4.5 and 0.75 kPa, respectively.

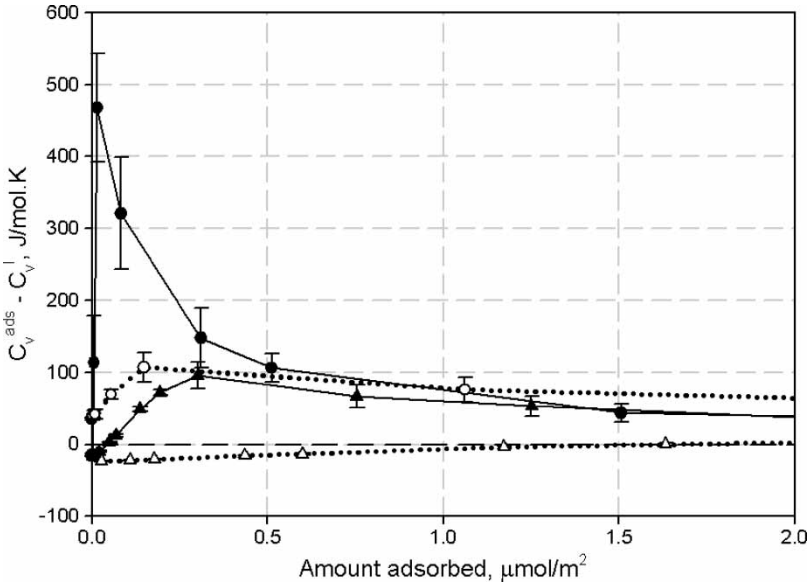

Figure 12. Deviation of the methanol adsorbed phase heat capacity (C_V^{ads}) from the saturated liquid heat capacity (C_V^l) versus loading for configurations: no carbonyls (filled circles with solid line), five carbonyls with $\delta = 0.3$ nm (filled triangles with solid line), 49 evenly spaced carbonyls (empty circles with dotted line) and nine groups of five carbonyls with $\delta = 0.3$ nm (empty triangles with dotted line). Lines are a guide for the eye only.

by equation (7).

$$\mathrm{CP} = \int_0^R g(r)\,\mathrm{d}r \tag{7}$$

where R is the upper limit of what is considered a cluster. Referring to figure 11, we can see that at low coverage the radial distributions are dominated by bonds up to 0.6 nm. This will be the limit, R, used in equation (7) for the calculation of the clustering parameter. The higher the value of CP, the greater the percentage of adsorbed molecules involved in isolated clusters of small numbers of molecules. Plots of the clustering parameter and heat capacity versus loading for a surface with no functional groups are given in figures 14 and 15 for methanol and ethanol, respectively.

The clustering parameter, CP, and heat capacity show a very strong correlation in figures 14 and 15 for both methanol and ethanol, respectively. Like the heat capacity, the CP increases at low loading to a sharp and obvious peak before decreasing as the amount adsorbed increases. The peak shows a preference for methanol and ethanol to form small and dispersed clusters on the surface. The most isolated clusters occur at the peak. At lower loadings, the incidence of hydrogen bonding decreases dramatically and at higher loading, the cluster either become larger or have neighbouring clusters increasingly close by. An isolated

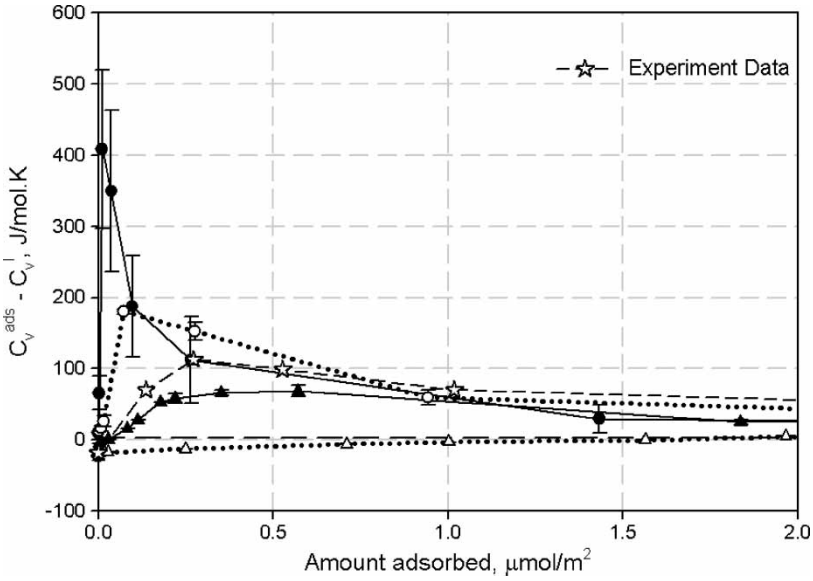

Figure 13. Deviation of the ethanol adsorbed phase heat capacity (C_V^{ads}) from the saturated liquid heat capacity (C_V^l) versus loading for configurations: no carbonyls (filled circles with solid line), five carbonyls with $\delta = 0.3$ nm (filled triangles with solid line), 49 evenly spaced carbonyls (empty circles with dotted line) and nine groups of five carbonyls with $\delta = 0.3$ nm (empty triangles with dotted line). Experimental data at 307.15 K [35] is represented by the empty stars with a dashed line. Lines are a guide for the eye only.

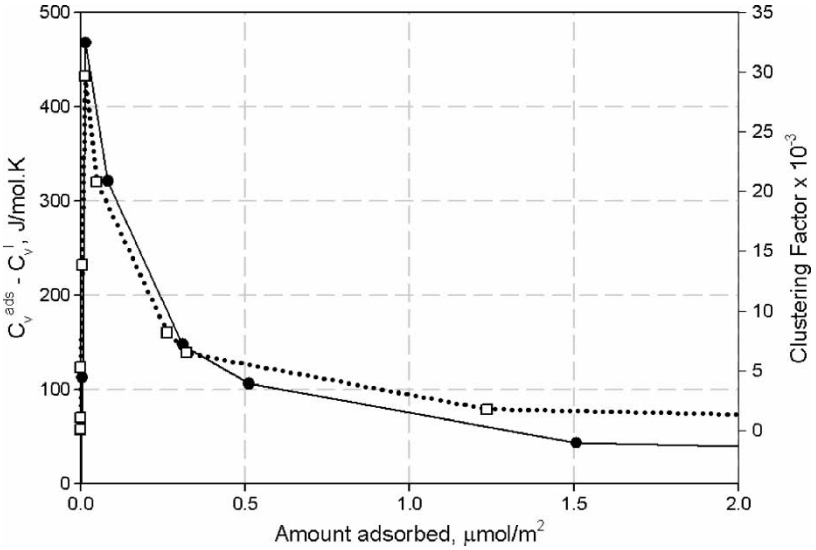

Figure 14. Deviation of the methanol adsorbed phase heat capacity (C_V^{ads}) from the saturated liquid heat capacity (C_V^l) versus loading for a surface with no functional groups (filled circles with solid line) and the clustering factor (as defined by equation (7)) versus loading (empty squares with dotted lines). Lines are a guide for the eye only.

cluster, upon heating, will have the greatest configurational energy loss (on a per molecule basis) due to the breaking of hydrogen bonds. When the loading is higher broken hydrogen bonds can be compensated by a larger number of alcohol molecules with which to potentially bond. At very low loading, there are no hydrogen bonds to be broken. At 300 K the calculation of the peak in CP and heat capacity requires a simulation box large enough to have a significant number of molecules in the simulation. At least 10 molecules are required in the simulation to give sufficient sampling of cluster configurations using AVB moves. Without a sufficiently sized box, the calculated amount adsorbed will be much the same but the heat capacity and clustering parameter at low loading can be in serious error. Even taking steps of using large simulation boxes and very long simulations (6×10^9 configurations), the variance of the heat capacities calculated is still very large in figures 12 and 13 for the case of a surface with no functional groups. Introducing heterogeneity to the surfaces decreases the importance of isolated clusters to the adsorption. In the case where high energy adsorption sites exist, like the grouped carbonyls, the reduction in the heat capacity will be the greatest.

The association of fluids on a homogeneous surface has been covered using classical theories by Kiselev and co-workers [37–39]. With these theories, isotherm, isosteric heat and heat capacity behaviour could be well approximated for associating fluids such as alcohols.

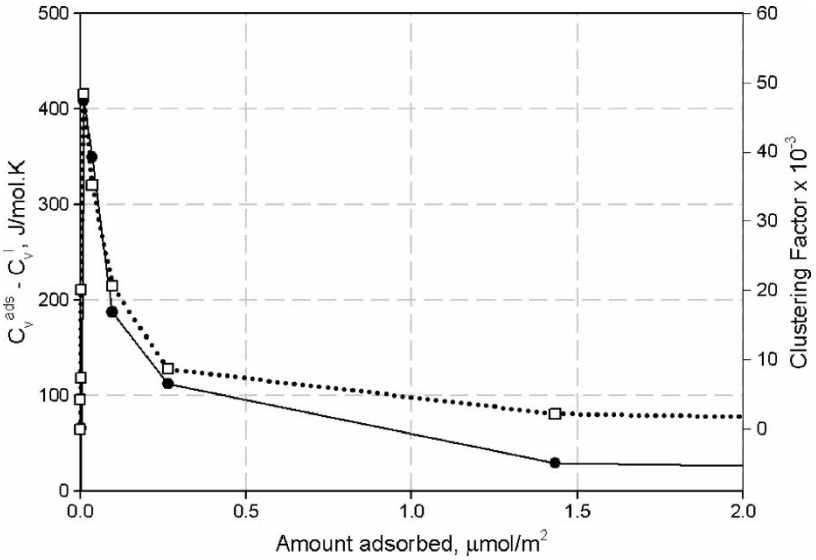

Figure 15. Deviation of the ethanol adsorbed phase heat capacity (C_V^{ads}) from the saturated liquid heat capacity (C_V^l) versus loading for a surface with no functional groups (filled circles with solid line) and the clustering factor (as defined by equation (7)) versus loading (empty circles with dotted lines). Lines are a guide for the eye only.

However, these theories did not take into account the effect of functional groups on the surface. This simulation study shows that for a perfect surface, the peak in the heat capacity is much greater than that seen in experiment. So whilst a classical theory can approximate what happens with experiment it does not reveal that the heat capacity is strongly affected by the heterogeneity of the surface and that this appears to be what occurs on even a highly graphitised carbon black [35].

5. Conclusions

Simulations for the adsorption of methanol and ethanol on graphitized thermal carbon black have been performed. The adsorption, up to monolayer coverage, and isosteric heats have been shown to be sensitive to functional groups on the surface. The methanol model used shows a good agreement with the experimental isotherms available in the literature. However, the agreement between the ethanol simulations and the literature isotherms is not as satisfactory. The adsorption of these alcohols has been shown to occur by forming two-dimensional clusters on the surface of the carbon. A neat tetramer structure has been shown to be prevalent in the adsorption prior to monolayer coverage. The association of the alcohols on the surface in fairly well defined structures leads to a maximum in the heat capacity. This maximum has been observed experimentally for ethanol in the literature but is greatly over predicted by the simulations when using a plain carbon surface. The maximum in the heat capacity is greatly reduced by the addition of carbonyls to the surface, even in concentrations as small as 0.09 carbonyls/nm^2, giving a more realistic heat capacity curve.

Acknowledgements

This research was made possible by the Australian Research Council whose support is gratefully acknowledged. Thanks also go to the University of Queensland High Performance Computing facility for a generous allocation of computing time.

References

[1] N. Metropolis, A.W. Rosenbluth, M.N. Rosenbluth, A.H. Teller, E. Teller. Equation-of-state calculations by fast computing machines. *J. Chem. Phys.*, **21**, 1087 (1953).
[2] D. Nicholson. A simulation study of energetic and structural heterogeneity in slit-shaped pores. *Langmuir*, **15**(7), 2508 (1999).
[3] M.B. Sweatman, N. Quirke. Modelling gas adsorption in slit-pores using Monte Carlo simulation. *Mol. Simul.*, **27**(5–6), 295 (2001).
[4] A. Striolo, A.A. Chialvo, P.T. Cummings, K.E. Gubbins. Water adsorption in carbon-slit nanopores. *Langmuir*, **19**(20), 8583 (2003).
[5] A. Striolo, K.E. Gubbins, A.A. Chialvo, P.T. Cummings. Simulated water adsorption isotherms in carbon nanopores. *Mol. Phys.*, **102**(3), 243 (2004).
[6] A. Striolo, K.E. Gubbins, M.S. Gruszkiewicz, D.R. Cole, J.M. Simonson, A.A. Chialvo. Effect of temperature on the adsorption of water in porous carbons. *Langmuir*, **21**(21), 9457 (2005).
[7] A. Striolo, A.A. Chialvo, K.E. Gubbins, P.T. Cummings. Water in carbon nanotubes: adsorption isotherms and thermodynamic properties from molecular simulation. *J. Chem. Phys.*, **122**(23), 234712 (2005).
[8] J.C. Liu, P.A. Monson. Does water condense in carbon pores? *Langmuir*, **21**(22), 10219 (2005).
[9] G.R. Birkett, D.D. Do. The adsorption of water in finite carbon pores. *Mol. Phys.*, **104**(4), 623 (2006).
[10] D.E. Ulberg, K.E. Gubbins. Water adsorption in microporous graphitic carbons. *Mol. Phys.*, **84**(6), 1139 (1995).
[11] E.A. Muller, L.F. Rull, L.F. Vega, K.E. Gubbins. Adsorption of water on activated carbons: a molecular simulation study. *J. Phys. Chem.*, **100**(4), 1189 (1996).
[12] C.L. McCallum, T.J. Bandosz, S.C. McGrother, E.A. Muller, K.E. Gubbins. A molecular model for adsorption of water on activated carbon: comparison of simulation and experiment. *Langmuir*, **15**(2), 533 (1999).
[13] M. Jorge, C. Schumacher, N.A. Seaton. Simulation study of the effect of the chemical heterogeneity of activated carbon on water adsorption. *Langmuir*, **18**(24), 9296 (2002).
[14] M. Jorge, N.A. Seaton. Characterisation of the surface chemistry of activated carbon by molecular simulation of water adsorption. *Studies Surf. Sci. Catal.*, **144**(VI), 131 (2002).
[15] A. Striolo, A.A. Chialvo, P.T. Cummings, K.E. Gubbins. Simulated water adsorption in chemically heterogeneous carbon nanotubes. *J. Chem. Phys.*, **124**(7), 074710 (2006).
[16] A.V. Shevade, S.Y. Jiang, K.E. Gubbins. Adsorption of water–methanol mixtures in carbon and aluminosilicate pores: a molecular simulation study. *Mol. Phys.*, **97**(10), 1139 (1999).
[17] A.V. Shevade, S.Y. Jiang, K.E. Gubbins. Molecular simulation study of water-methanol mixtures in activated carbon pores. *J. Chem. Phys.*, **113**(16), 6933 (2000).
[18] B. Chen, J.J. Potoff, J.I. Siepmann. Monte Carlo calculations for alcohols and their mixtures with alkanes. Transferable potentials for phase equilibria. 5. United-atom description of primary, secondary, and tertiary alcohols. *J. Phys. Chem. B*, **105**(15), 3093 (2001).
[19] T. Schnabel, J. Vrabec, H. Hasse. Henry's law constant of methane, nitrogen, oxygen and carbon dioxide in ethanol from 273 K to 498 K: prediction from molecular simulation. *Fluid Phase Equilib.*, **233**, 134 (2005).
[20] A.Z. Panagiotopoulos. Direct determination of phase coexistence properties of fluids by Monte Carlo simulation in a new ensemble. *Mol. Phys.*, **61**(4), 813 (1987).
[21] A.Z. Panagiotopoulos, N. Quirke, M. Stapleton, D.J. Tildesley. Phase equilibria by simulation in the Gibbs ensemble. Alternative derivation, generalization, and application to mixture and membrane equilibria. *Mol. Phys.*, **63**(4), 527 (1988).
[22] W.A. Steele. Physical interaction of gases with crystalline solids. I. Gas–solid energies and properties of isolated adsorbed atoms. *Surf. Sci.*, **36**(1), 317 (1973).
[23] M. Jorge, N.A. Seaton. Molecular simulation of phase coexistence in adsorption in porous solids. *Mol. Phys.*, **100**(24), 3803 (2002).
[24] W.L. Jorgensen, J. Tirado-Rives. The OPLS (optimized potentials for liquid simulations) potential functions for proteins, energy minimizations for crystals of cyclic peptides and crambin. *J. Am. Chem. Soc.*, **110**(6), 1657 (1988).
[25] G.R. Birkett, D. Do. Simulation study of ammonia adsorption on graphitised carbon black. *Mol. Simul.*, **32**(7), 523 (2006).
[26] T. Morimoto, K. Miura. Adsorption sites for water on graphite. 1. Effect of high-temperature treatment of sample. *Langmuir*, **1**(6), 658 (1985).
[27] T. Morimoto, K. Miura. Adsorption sites for water on graphite. 2. Effect of autoclave treatment of sample. *Langmuir*, **2**(1), 43 (1986).
[28] M.P. Allen, T.P. Tildesley. *Computer Simulation of Liquids*, Clarendon Press, Oxford (1987).
[29] B. Chen, J.I. Siepmann. Improving the efficiency of the aggregation-volume-bias Monte Carlo algorithm. *J. Phys. Chem. B*, **105**(45), 11275 (2001).
[30] D.M. Heyes, F. Van Swol. The electrostatic potential and field in the surface region of lamina and semi-infinite point charge lattices. *J. Chem. Phys.*, **75**(10), 5051 (1981).
[31] M. Jorge, N.A. Seaton. Long-range interactions in Monte Carlo simulation of confined water. *Mol. Phys.*, **100**(13), 2017 (2002).
[32] D.M. Heyes, M. Barber, J.H.R. Clarke. Molecular dynamics computer simulation of surface properties of crystalline potassium

chloride. *J. Chem. Soc. Faraday Trans. 2*, Mol. Chem. Phys. **73**(10), 1485 (1977).
[33] D. Nicholson. A simulation study of energetic and structural heterogeneity in slit-shaped pores. *Langmuir*, **15**(7), 2508 (1999).
[34] N.N. Avgul, A.V. Kiselev. Physical adsorption of gases and vapors on graphitized carbon blacks. *Chem. Phys. Carbon*, **6**, 1 (1970).
[35] G.I. Berezin, A.V. Kiselev, I.V. Kleshnina. Heat capacities of alcohols adsorbed on graphitised carbon black. *Russ. J. Chem. Phys.*, **43**, 2946 (1969).
[36] G.I. Berezin, A.V. Kiselev, R.T. Sagatelyan, O.S. Chistozvonova. Adsorption of ethanol on the surface of graphitised carbon black at different temperatures. *Russ. J. Phys. Chem.*, **46**(3), 432 (1972).
[37] G.I. Berezin, A.V. Kiselev. Variation of heats of adsorption and heat capacity of adsorbate with surface coverage. 2. Localised adsorption with adsorbate–adsorbate interaction. *Russ. J. Phys. Chem.*, **42**(8), 1045 (1968).
[38] G.I. Berezin, A.V. Kiselev. Adsorbate–adsorbate association on a homogeneous surface of a non-specific adsorbent. *J. Colloid Interface Sci.*, **38**(2), 227 (1971).
[39] G.I. Berezin, A.V. Kiselev, R.T. Sagatelyan, V.A. Sinitsyn. A thermodynamic evaluation of the state of the benzene and ethanol on a homogeneous surface of a nonspecific adsorbent. *J. Colloid Interface Sci.*, **38**(2), 335 (1971).